Calibration of atomic force microscope cantilevers based on μ-LDV: Metrological insight on the constitutive experimental parameters of Sader's formula for spring constant

Measurement: Sensors 38 (2025) 101744

Contents lists available at ScienceDirect

Measurement: Sensors

journal homepage: www.sciencedirect.com/journal/measurement-sensors

Calibration of atomic force microscope cantilevers based on μ-LDV: Metrological insight on the constitutive experimental parameters of Sader's formula for spring constant

ARTICLE INFO

Keywords:
Metrological AFM
Sader's formula
μ-LDV
Cantilevers
Spring constant
Uncertainties

ABSTRACT

This paper investigates the experimental parameters of the Sader's formula, to calculate the spring constant of cantilevers used in Atomic Force Microscopy (AFM), with the related detailed uncertainty budget. Recently, a significant update of the metrological AFM is underway at INRiM, in order to provide traceable and accurate measurements of material properties at nano-scale level. While a procedure to provide the metrological traceability to SI for nano-scale displacements, in the horizontal X-axis and Y-axis plane, and along the vertical Z-axis was established, a procedure for the nanoscale force traceability is still lacking. Due to the impossibility to provide direct traceability to force at the micro- and nano-scale level, an indirect method is exploited, by extracting nano-force values, from the spring constant of the cantilever. Based on micro Laser Doppler Velocimetry measurements, the elastic properties of cantilevers are derived, by measuring the fundamental resonant frequency and damping of free oscillations, according to Sader's approach.

1. Introduction

Atomic force microscopy (AFM) is nowadays widely applied in material science for imaging surfaces, measuring properties, and manipulating matter at the nanoscale level. In very general terms, the principle of functioning of AFM can be summarized in terms of Hooke's law: the occurring dragging forces between the probe-tip (supported by a flexible cantilever) and the sample under investigation generate deflections of the cantilever, revealing the topographical, morphological or rheological properties of the sample itself. AFM can operate in static modes (contact, with cantilever deflections), for force spectroscopy (contact, with dynamic force-displacement interaction between cantilever and sample), and dynamic modes (non-contact or "tapping", with cantilever oscillations).

Therefore, an accurate determination of the elastic properties of these cantilevers is of fundamental importance for the actualization of a functional metrological AFM. This is done to improve the reliability of quantitative information and experimental evidence, and to provide a "provisional" traceability to measurement results, at least until the force-scale traceability is extended down to micro- and nano-scale.

In literature, among several methods proposed to evaluate the cantilever spring constant, Sader's approach is probably one of the most detailed, as well as most popular [1–4]. In this paper, as a case study, the constitutive parameters of the Sader's formula are experimentally determined, along with a detailed analysis of the uncertainty budget and propagation. The dynamic vibrational response, in terms of resonant frequency and damping, and the geometrical dimensions of a single AFM cantilevers are investigated using micro Laser Doppler Velocimetry technique (μ-LDV) and scanning electron microscopy (SEM); in addition, the impact of hydrodynamic effects of the surrounding fluid (whose fundamental physical properties are derived according to Rasmussen's model [5]) on the determination of the spring constant is investigated. The proposed analysis aims to investigate some assumptions supporting the metrological traceability of measurements based on AFM.

1.1. A metrological AFM

A functional metrological AFM is expected to provide traceable and accurate quantification of material properties at the nano-scale level. Metrological AFM, usually developed in the NMIs, allows quantifying the in-plane and out-of-plane topographical, dimensional and morphological properties of nanoparticles and nanostructures of different nature (with sub-nanometer accuracy), by using interferometric systems, to provide measurements of the tip–sample relative positions, traceable to SI [6–9]. However, the rheological properties of materials (estimated from the force-displacement interaction between cantilever and sample), can only be attributed in a partially quantitative form, since force traceability to SI at the nano-scale is still missing. To make up for this lack, occurring forces at the nano-scale are indirectly traced back from the elastic properties of the cantilevers. At present, calibrations of AFM cantilevers are supplied by the Global Calibration Initiative tool, that combines Sader and thermal methods, along with an estimation of relative standard uncertainty, directly comparing calibration results with the worldwide AFM community users [10–12]. In this perspective at INRiM, an accurate method to individually calibrate AFM cantilevers, based on dynamic measurement of free oscillations, based on μ-LDV technique, is investigated.

1.2. Calibration of AFM cantilever

Although term "calibration" is not properly suitable for the evaluation of elastic properties of the cantilevers (it would be more appropriate

https://doi.org/10.1016/j.measen.2024.101744

Available online 2 January 2025

to refer in terms of "metrological characterization"), hereinafter we will use "calibration", for compliance purposes only, as commonly used by the AFM community users. In the technical and scientific literature, over the last three decades, several theoretical and experimental methods have been proposed and developed to calibrate AFM cantilevers, from the evaluation of the related spring constant. The methodologies can be summarized in three main categories:

1) The dimensional methods, based on the measurement of the geometrical properties of the cantilever via dimensional methods [13].
2) The static experimental methods, based on the direct measurement of reference properties, such known masses attached on the cantilever tip, or pendulum law [14].
3) The dynamic methods, based on the cantilever's resonant response and accurate measurement of the cantilever's plan view dimensions [15]. The most widely used techniques are: Cleveland method [13], Sader method [3], and thermal noise method [16].

In this context, we do not discuss or compare different methods, referring the reader to the relevant bibliographic references [17–20]. Nevertheless, after a careful analysis, the Sader's approach appears as the most well-structured and accurate, from a physical point of view. Indeed, all the boundary conditions of the general theory of the dynamic behaviour of a beam (independently of its shape) immersed in a viscous fluid, and excited by an external driving force, are detailed taken into account.

2. Methods and procedures

The spring constant k_S of a commercial AFM cantilever (type: HQ: NSC14/AlBS, manufactured by MikroMasch® [21]) is determined on the basis of Sader's formula (1), connecting the dynamic spring constant to the dissipative properties of the cantilever at resonance. The constitutive parameters of the Sader's formula are experimentally determined, namely the geometrical dimensions of the cantilevers, in terms of length and width, are measured by means of scanning electron microscopy (SEM), and the dynamical vibrational response, in terms of resonance and damping, is measured by means of micro Laser Doppler Velocimetry technique (μ-LDV); moreover, the hydrodynamic effects of the surrounding fluid in which the cantilever is immersed, affecting the dynamic behaviour of the cantilever itself, are investigated. To take into account these effects on the spring constant calculation, the hydrodynamic function is opportunely calculated, according to the environmental conditions of the fluid during the test and to the shape of the cantilever examined.

Finally, the detailed uncertainty budget of the Sader's formula is established, on the basis of the general rule of random error propagation, according to Guide to the Expression of Uncertainty in Measurement (GUM) [22].

2.1. Sader's formula

Without delving into the theoretical background of the analytical demonstration, on which the formulation is based [1–4], the fundamental generalized result of Sader for the determination of cantilevers spring constant k_S, converges as follows:

$$k_S = 0.1906\, b^2\, L\, \rho_{air}\, \Gamma_{i,rect}(\omega_0)\, \omega_0^2\, Q_0, \tag{1}$$

where b is the cantilever width (m), L is the cantilever length (m), ρ_{air} is the fluid (air) density (kg·m^{-3}), $\Gamma_{i.rect}(\omega_0)$ is the imaginary part of the hydrodynamic function for the rectangular beams, ω_0 is the fundamental resonance frequency of the cantilever in air (rad·s^{-1}), and Q_0 is the quality factor of the fundamental resonance frequency in air.

As is possible to notice from (1), the spring constant k_S of the cantilever depends on two dimensional quantities, such as the width b, and the length L (and it is independent from its thickness), and on two dynamic quantities, such as the resonance frequency of free oscillation ω_0 (in air with density ρ_{air}), and its quality factor Q_0; a little tricky is the calculation of hydrodynamic function, as well as related uncertainties.

The hydrodynamic complex function for the rectangular beams $\Gamma_{rect}(\omega_0)$, is derived from the exact analytical form of hydrodynamic complex function for circular beams $\Gamma_{circ}(\omega_0)$, adjusted under several assumptions, by a correction complex function $\Omega(\omega_0)$, in the following form:

$$\Gamma_{rect}(\omega_0) \cong \Omega(\omega_0)\Gamma_{circ}(\omega_0), \tag{2}$$

The hydrodynamic complex function for circular beams $\Gamma_{circ}(\omega_0)$, is given by:

$$\Gamma_{circ}(\omega_0) = 1 + \frac{4iK_1\left(-i\sqrt{i\mathrm{Re}}\right)}{\sqrt{i\mathrm{Re}}K_0\left(-i\sqrt{i\mathrm{Re}}\right)}, \tag{3}$$

where K_0 and K_1 are the modified Bessel function of the third kind, in which the variable is $-i\sqrt{i\mathrm{Re}}$, where Re is the Reynold's number, calculated as:

$$\mathrm{Re} = \frac{\rho_{air}\omega_0 b^2}{4\mu_{air}}, \tag{4}$$

where μ_{air} is the fluid (air) dynamic viscosity (Pa·s), and b is the width of the cantilever (assumed as the dominant length scale in the flow, i.e., for circular beams it corresponds to the diameter), other parameters were defined in (1).

Both air density ρ_{air} and air dynamic viscosity μ_{air} are determined by applying the detailed Rasmussen's formula, currently used in microphone calibration procedures [5]. Rasmussen's formula allows calculating the air properties as function of measured air temperature T (K), relative humidity RH (%), and air pressure p_0 (Pa), taking into account the effects of each relevant gas properties.

In order to approximate the exact analytical solution for circular beams to a suitable solution for rectangular beams, the following correction function is introduced:

$$\Omega(\omega_0) = \Omega_r(\omega_0) + i\Omega_i(\omega_0), \tag{5}$$

$\Omega(\omega_0)$ is expressed as a rational function in $\log_{10}$Re, which satisfies the asymptotic conditions $\Omega(\omega_0) \to 1$ as Re$\to$0 and Re$\to\infty$. The unknown coefficients in the rational function are evaluated from a nonlinear least-squares fit regression of sixth order function, that can be summarized as:

$$\Omega_r(\omega_0) = \left(\sum_{n=0}^{6} A_n \tau^n\right)\left(\sum_{n=0}^{6} (B_n \tau^n)^{-1}\right), \tag{6}$$

$$i\Omega_i(\omega_0) = i\left(\sum_{n=0}^{6} (C_n \tau^n)\right)\left(\sum_{n=0}^{6} (D_n \tau^n)^{-1}\right), \tag{7}$$

where the numerical coefficients of the fit regression A_n, B_n, C_n and D_n, are explicitly provided in Ref. [2], and $\tau = \log_{10}\mathrm{Re}$.

2.2. Experimental analysis

Dimensional quantities of the cantilevers are determined from SEM micrographies, as shown in Fig. 1, analysed by means of a tabletop SEM Hitachi TM3000. The images of the cantilever (measured at different magnifications 250x, 500x and 800x with an accelerating voltage of 15 kV) are analysed by extrapolating the length L and width b in pixels.

The standard deviation of L and b is calculated on the basis of by multiple repetitions of width and length profiles, namely 4 repetition of length and 24 repetitions of width. Afterwards, in order to calibrate the pixel size, with the same magnifications was measured a grid sample, previously calibrated by means of an optical diffractometer, whose He-

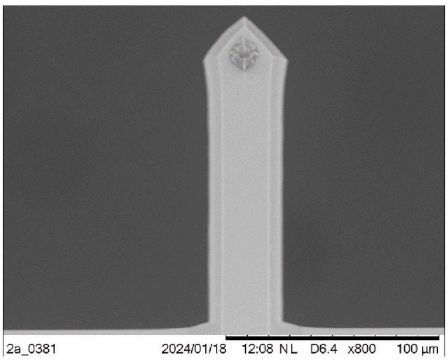

Fig. 1. SEM micrograph of the cantilever HQ:NSC14/AlBS (800x).

Ne laser source is calibrated against the INRiM *MeP* frequency-stabilized laser meter. In this way, using the coefficients [µm/pixel] from the calibration grid, the length L and width b are accurately expressed in µm, and traceable to SI. To extract these parameters, the metrology software Digital Surf MountainsSPIP [23], is used.

Dynamic quantities are determined by measuring the resonance frequency ω_0 and the quality factor of the cantilever Q_0, by using a µ−LDV, namely a Polytec laser Doppler vibrometer based on VibroFlex Connect front and VibroFlex Compact sensor, with integrated camera and VIB-A-20XLENS microscope lens. The cantilever is fixed on a proper support opportunely designed and realized, the µ−LDV is placed on an active anti-vibration table.

The measurement of the resonance frequency ω_0 and the quality factor of the cantilever Q_0, are performed along the length of the cantilever in 4 different equidistant positions (both in the front and in the rear). Measurements are performed in air, by accurately monitoring the environmental temperature, relative humidity and static pressure. The frequency response of the cantilever is determined by using the Brownian motion of the molecules in the surrounding fluid as thermal driving force. Any dissipative effects due to internal frictional losses in the beam are assumed to be negligible in comparison to those exhibited by the fluid. Since these conditions are typically satisfied in AFM cantilever beams [16,24–27], results here presented directly give the thermal noise spectra of the cantilever. In Fig. 2, the µ−LDV and a single point measurement are shown.

The frequency analysis is carried out by using a NI PXIe-1071, with a sampling rate of 1 MHz, and 1 Hz of resolution.

The standard deviation of ω_0 and Q_0 is calculated on the basis of 200 averaged spectra, for each single point of measurement. In Fig. 3, as an example, the averaged thermal noise spectra, related to 4 positions along the length of the cantilever here investigated, is depicted.

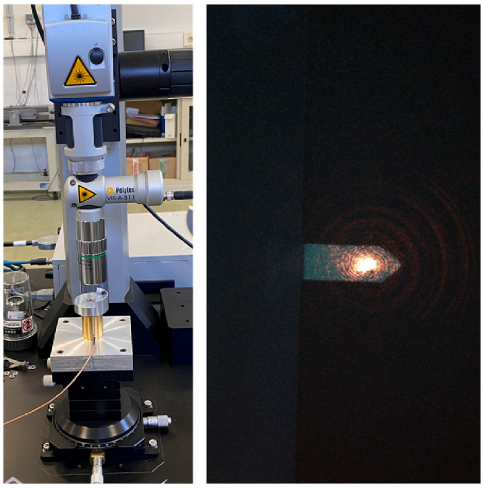

Fig. 2. The µ−LDV and a single point measurement (laser spot diameter ~ 1.5 µm) on the cantilever HQ:NSC14/AlBS (20x objective).

As is possible to notice from Fig. 3, the resonant peak and its width, are clearly defined (1 Hz of resolution). The peak amplitude proportionally increases as the measurement is performed close to tip of the cantilever, as expected for a beam with clamped and free end conditions; namely, the maximum amplitude displacement (at the tip) is ~0.7 µm.

2.3. Uncertainty budget definition

An in-depth analysis of uncertainty budget, is expected to provide useful information with the aim to improve the measurement precision of AFM cantilever spring constant, supporting the "provisional" force traceability at nanoscale.

The definition of the detailed uncertainty budget of Sader's formula (1), is calculated, according to GUM. The related expanded uncertainty, with a confidence level of 95 % (coverage factor $k = 2$) of the spring constant $U(k_S)$, is determined as follows:

$$U(k_S) = 2\sqrt{\sum_{i=1}^{N}\left(\frac{\partial k_S}{\partial x_i}\right)^2 u^2(x_i)}, \tag{7}$$

where x_i is the ith independent variable of Sader's formula, and $u^2(x_i)$ is the standard uncertainty associated to the independent variable x_i.

Each single constitutive parameter of Sader's formula, is individually expressed with the related uncertainty $u(x_i)$, the coefficient of sensitivity $\left(\frac{\partial k_S}{\partial x_i}\right)$, and the resulting squared combined uncertainty $u_c^2(y) = \left(\frac{\partial k_S}{\partial x_i}\right)^2 u^2(x_i)$.

The values of standard uncertainties, $u^2(x_i)$, are calculated either as the square of the experimental standard deviation if the quantity randomly varies (type An uncertainty), or as the square of half-width of the interval of variability (divided by 3, considering a rectangular distribution) if the quantity is obtained from the manufacturer's specifications and calibration certificates (type B uncertainty).

As previously reported, dimensional quantities and dynamic quantities are determined from repeated measurements, as a function of its intrinsic variability, then as type An uncertainty; quantities related to the air properties (i.e., the surrounding fluid in which the cantilever is immersed), are determined by propagating type B uncertainties. Properly, air temperature (T), relative humidity (RH), and static atmospheric pressure (p_s), are provided according the instruments proper resolution.

The uncertainties related to the air properties, specifically air density ρ_{air} and air dynamic viscosity μ_{air}, are propagated to estimate the Reynold's number, equation (4), that in turn allows to build the variability of the hydrodynamic function $\Gamma_{circ}(\omega_0)$, equation (3), and the variability of the correction function $\Omega(\omega_0)$, equations (5)–(7), for the

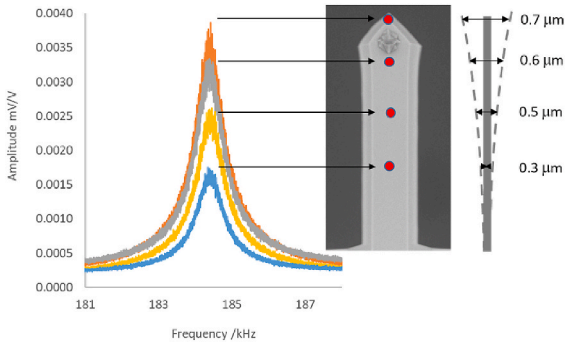

Fig. 3. The frequency response of the cantilever HQ:NSC14/AlBS, thermally excited, extracted from draft data of frequency analysis, and the related mechanical behavior.

approximation to the hydrodynamic function for the rectangular beams, i.e., $\Gamma_{\mathrm{rect}}(\omega_0) \cong \Omega(\omega_0)\Gamma_{\mathrm{circ}}(\omega_0)$.

According to Rasmussen's model, we calculate the air density from:

$$\rho_{\mathrm{air}} = 3.48349 \cdot 10^{-3} \cdot \frac{p_s}{ZT}\,(1 - 0.378 \cdot x_w), \tag{8}$$

and air dynamic viscosity from:

$$\mu_{\mathrm{air}} = \left(a_0 + a_1 T + (a_2 + a_3 T)x_w + a_4 T^2 + a_5 x_w^2\right) \cdot 10^{-8}, \tag{9}$$

where the numerical parameters a_n are explicitly provided in Ref. [5], as well as the calculation model of the mole fraction of water vapor in air x_w, as a function of experimental relative humidity RH, static pressure p_s, enhancement factor $f(p_s, T)$, and saturation water vapor pressure $p_{sv}(T)$; and the calculation model of compressibility factor $Z(p_s, T, x_w)$.

In the following flowchart, the complete set of relationships, among constituent parameters of Sader's formula, along with Rasmussen's model, are then summarized:

As shown in the flowchart of Fig. 4, experimental measured quantities are collected in green boxes. Environmental parameters, i.e., air temperature T, static atmospheric pressure p_s, and relative humidity RH, allows calculating both air density ρ_{air} and air dynamic viscosity μ_{air}, by considering all constitutive gas properties, as previously described. Uncertainties are then propagated to estimate the expanded uncertainty of the Reynold's number; moreover, the uncertainty of air density is directly propagated for the estimation of the elastic constant k_S. The uncertainties of dimensional quantities, i.e., length L and width b, are propagated toward the elastic constant; width b is propagated also toward Reynold's number. The uncertainties of dynamic quantities, i.e., quality factor Q_0 is propagated directly to the elastic constant, while the resonance frequency ω_0, is propagated to both elastic constant and Reynold's number. Once the expanded uncertainty of Reynold's number is evaluated, the expanded uncertainty of the hydrodynamic function $\Gamma_{\mathrm{circ}}(\omega_0)$, equation (2), and of the correction function $\Omega(\omega_0)$, equation (3), are calculated as well, in order to provide the related expanded uncertainty to the hydrodynamic function for rectangular beams, calculated as $\Gamma_{\mathrm{rect}}(\omega_0) \cong \Omega(\omega_0)\Gamma_{\mathrm{circ}}(\omega_0)$. The whole set of the expanded uncertainties of the constative parameters of Sader's formula are then propagated to calculate the expanded uncertainty of the elastic constant k_S.

As it will be shown in the next Section 3, a detailed analysis of the coefficient of sensitivities is carried out, for each single parameter, in order to estimate the major uncertainty contributions, and to provide possible solutions for the mitigation.

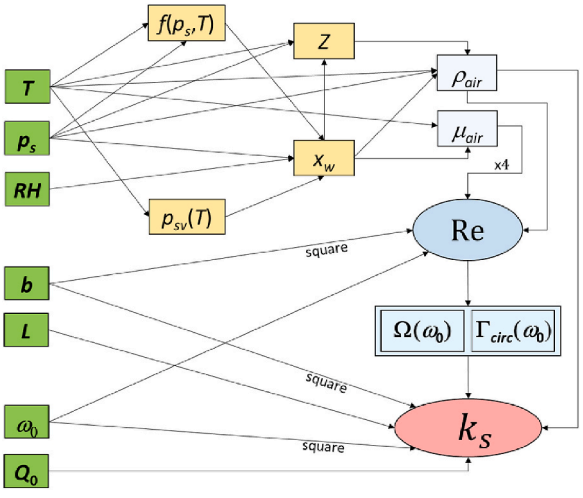

Fig. 4. Flowchart of Sader's parameters relationships.

3. Results and discussion

The experimental parameters (indicated in green boxes in the flowchart of Fig. 4) are summarized in Table 1, with related uncertainty, type of uncertainty and percentage. The frequency f_0 is expressed in Hz, namely the angular frequency is simply calculated as $\omega_0 = 2\pi f_0$, while the environmental temperature T is expressed in °C, then the temperature in Kelvin is calculated by adding 273.15 K.

As a first step, according to GUM by applying the rules of equation (7), deriving the Rasmussen model with respect its independent variables, the uncertainties of air density and air viscosity are calculated. In Table 2 are indicated the resulting values, the related uncertainty, and the percentage, of air properties.

The uncertainties of dimensional quantities, are calculated from repeated measurement of length and width, performed using SEM.

The uncertainties of dynamical quantities are determined after 8 repetitions along the length of the cantilever (upper side and bottom side). While resonance frequency is very stable (results are strongly repeatable), the values of quality factor (calculated as $Q_0 = f_0/\Delta f_{-3\mathrm{dB}}$) show larger dispersions, both in terms of repeatability and accuracy. As shown in Fig. 5, the determination of Q_0 is affected by several uncertainties due to the experimental data dispersion. Indeed, although in first analysis, is possible to fit the resonance peak with suitable functions (e.g., Lorentzian function), is not possible to accurately establish A_{MAX}, (then the corresponding half-power points), and the intersection points to uniquely evaluate the width of $\Delta f_{-3\mathrm{dB}}$. Since the resonance peak is extremely narrow, even small deviations on amplitude dA, and on frequency df, lead to large variations in the estimation of the actual width of the resonance peak.

To avoid effects due to the thermal noise spectra [28], Sader suggest to use a formula allowing to calculate the true quality factor Q_{true} allowing to reduce the uncertainty from ~10 % (see Table 1) down to ~1 % [29], by applying the following relation:

$$Q_{\mathrm{true}} = \frac{\pi f_0}{2\delta f}\left(1 - \sqrt{1 - Q_0 \frac{4\delta f}{\pi f_0}}\right), \tag{10}$$

where δf is the frequency division from the discrete Fourier transform.

The uncertainties of the experimental parameter are then exploited to evaluate the uncertainty of the Reynold's number, and consequently, to propagate the uncertainties into the imaginary part of the hydrodynamic function for the rectangular beams, calculated according equation (2). Values are reported in the following Table 3.

Once the whole set of experimental data, along with uncertainties, and the related propagation into hydrodynamic function is known, it is possible to calculate the spring constant k_S (in N/m) of the cantilever, along with the proper expanded uncertainty.

In the following Table 4, the detailed uncertainty budget, including the associated standard uncertainty, the coefficients of sensitivity, and the squared combined uncertainty of the spring constant of the

Table 1
Experimental parameters and uncertainties.

	Value	Unit	Standard Unc.	Type	%
T	22.9	°C	$5.8{\cdot}10^{-2}$	B	0.25
p_s	99590	Pa	28.87	B	0.03
RH	54.6	%	3.15	B	5.77
b	$3.34{\cdot}10^{-5}$	m	$5{\cdot}10^{-7}$	A	1.50
L	$14.5{\cdot}10^{-5}$	m	$3{\cdot}10^{-7}$	A	0.21
f_0	184393	Hz	23	A	0.01
Q_0	276.94	–	30.91	A	11.2

Table 2
Uncertainty budget of air density and air viscosity.

	Value (x_i)	Unit	$u(x_i)$	%
ρ_{air}	1.16545	kg·m^{-3}	5.7·10^{-4}	0.05
μ_{air}	1.82582·10^{-5}	Pa·s	3.2·10^{-9}	0.02

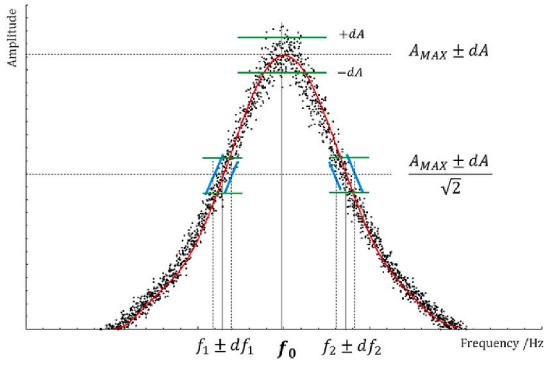

Fig. 5. Experimental values of the cantilever resonance and the method applied for quality factor estimation.

Table 3
Uncertainty budget of Reynold's number and of imaginary part of the hydrodynamic function.

	Value (x_i)	$u(x_i)$	$k \cdot u(x_i)$	%
Re	20.625	0.62	1.26	2.99
$\Gamma_{i,rect}(\omega_0)$	0.7065	6.8·10^{-3}	1.4·10^{-2}	1.92

investigated cantilever, as described in Section 2.3, are shown.

As shown in Table 4, the resulting spring constant of the cantilever investigated is $k_S = 9.44 \pm 0.68$ N/m. It should be noted that relation (1) also contains the constant term 0.1906. This term is related the normalized effective mass, derived from the length scale of the cantilever, as the Rayleigh quotient of the Rayleigh-Ritz method, by conservation of energy. The expanded uncertainty (calculated by taking into account all possible sources of uncertainties, at a confidence level of 95 %), indicates that the spring constant of this AFM cantilever can be accurately determined within 7.23 %. This evidence implies that occurring dragging force acting on the AFM cantilever can be estimated with an uncertainty of about 7 %, at least on the basis of the present analysis.

As is possible to notice, according to the detailed budget of uncertainty, the contributions having the greatest influence on the measurement of the spring constant k_s of the cantilever here investigated, are mainly related to the determination of true quality factor Q_{true}, and to the width of the cantilever b. Nevertheless, as observed, the evaluation of Q_{true} is also affected by a low repeatability, depending on measurement point position, as a consequence in-depth investigations of methods to mitigate the related dispersion are needed.

4. Conclusions

In this paper a detailed uncertainty budget of the constitutive parameters of Sader's formula, for the determination of the elastic constant of a commercial AFM cantilever (type: HQ:NSC14/AlBS, manufactured by MikroMasch®), is investigated. Each parameter is experimentally measured, along with the related proper uncertainty. Dimensional quantities of the cantilever are determined from repeated measurement of length and width, by means of Scanning Electron Microscope (SEM),

Table 4
Detailed uncertainty budget of the spring constant of the investigated cantilever.

	Value (x_i)	$u^2(x_i)$	$\left(\frac{\partial k_S}{\partial x_i}\right)$	$u_c^2(y)$
b	3.34·10^{-5}	2.5·10^{-13}	5.7·10^{5}	8.0·10^{-2}
L	14.5·10^{-5}	9.0·10^{-14}	6.5·10^{4}	3.8·10^{-4}
ρ_{air}	1.16545	3.2·10^{-7}	8.1	2.1·10^{-5}
f_0	184393	5.3·10^{2}	1.4·10^{-4}	5.6·10^{-6}
Q_{true}	276.9	9.6	3.4·10^{-2}	1.1·10^{-2}
$\Gamma_{i,rect}(\omega_0)$	0.7065	1.4·10^{-4}	1.3	2.5·10^{-2}
k_S	**9.44 N/m**			
Variance: $\sum u_c^2(y)$				0.12
Uncertainty: $\sqrt{\sum u_c^2(y)}$				0.34
Degrees of freedom: $\left(\sum u_c^2(y)\right)^2 / \left(\sum u_c^4(y)/\nu_i\right)$				56
Confidence level				95.0 %
Coverage factor k				2.0
Expanded uncertainty: $k \cdot u(y)$				**0.68**

and dynamic quantities, namely resonance frequency and quality factor, are determined from repeated measurement by using a micro Laser Doppler Velocimetry (μ−LDV) technique. Moreover, the uncertainties of the hydrodynamic function (only dependent from Reynold's number) are investigated as well, by propagating the uncertainties from the Rasmussen model, applied to accurately calculate the air properties.

Acknowledgments

Project funded under the National Recovery and Resilience Plan (NRRP), Mission 04 Component 2 Investment 3.1 – NextGenerationEU, Call for tender n. 3264 dated 28/12/2021.

Award Number: 128 dated 21/06/2022 – Project Code: IR0000027 - iENTRANCE@ENL: Infrastructure for Energy TRAnsition aNd Circular Economy @ EuroNanoLab.

References

[1] J.E. Sader, I. Larson, P. Mulvaney, L.R. White, Method for the calibration of atomic force microscope cantilevers, Rev. Sci. Instrum. 66 (7) (1995) 3789–3798.
[2] J.E. Sader, Frequency response of cantilever beams immersed in viscous fluids with applications to the atomic force microscope, J. Appl. Phys. 84 (1) (1998) 64–76.
[3] J.E. Sader, J.W. Chon, P. Mulvaney, Calibration of rectangular atomic force microscope cantilevers, Rev. Sci. Instrum. 70 (10) (1999) 3967–3969.
[4] J.E. Sader, J.A. Sanelli, B.D. Adamson, J.P. Monty, X. Wei, S.A. Crawford, E. J. Bieske, Spring constant calibration of atomic force microscope cantilevers of arbitrary shape, Rev. Sci. Instrum. 83 (10) (2012).
[5] K. Rasmussen, Calculation Methods for the Physical Properties of Air Used in the Calibration of Microphones, Report No. PL-11b, Technical University of Denmark, Lyngby, Denmark, 1997.
[6] G.B. Picotto, M. Vallino, L. Ribotta, Tip–sample characterization in the AFM study of a rod-shaped nanostructure, Meas. Sci. Technol. 31 (8) (2020) 084001.
[7] R. Bellotti, G.B. Picotto, L. Ribotta, AFM measurements and tip characterization of nanoparticles with different shapes, Nanomanufact. Metrol. 5 (2) (2022) 127–138.
[8] V. Maurino, F. Pellegrino, G.B. Picotto, L. Ribotta, Quantitative three-dimensional characterization of critical sizes of non-spherical TiO_2 nanoparticles by using atomic force microscopy, Ultramicroscopy 234 (2022) 113480.
[9] L. Ribotta, Dimensional Metrology at the Nanoscale: Quantitative Characterization of Nanoparticles by Means of Metrological Atomic Force Microscopy, PhD Dissertation, Politecnico di Torino, 2022.
[10] J.E. Sader, in: A. Hubbard (Ed.), Encyclopedia of Surface and Colloid Science, Dekker, New York, 2002, pp. 846–856.
[11] J.E. Sader, R. Borgani, C.T. Gibson, D.B. Haviland, M.J. Higgins, J.I. Kilpatrick, T. Zheng, A virtual instrument to standardise the calibration of atomic force microscope cantilevers, Rev. Sci. Instrum. 87 (9) (2016).
[12] See https://sadermethod.orgforGCI.
[13] J.P. Cleveland, S. Manne, D. Bocek, P.K. Hansma, A nondestructive method for determining the spring constant of cantilevers for scanning force microscopy, Rev. Sci. Instrum. 64 (2) (1993) 403–405.
[14] C.A. Clifford, M.P. Seah, Improved methods and uncertainty analysis in the calibration of the spring constant of an atomic force microscope cantilever using static experimental methods, Meas. Sci. Technol. 20 (2009) 125501.
[15] A.D. Slattery, J.S. Quinton, C.T. Gibson, Atomic force microscope cantilever calibration using a focused ion beam, Nanotechnology 23 (2012) 285704.
[16] J.L. Hutter, J. Bechhoefer, Calibration of atomic-force microscope tips, Rev. Sci. Instrum. 64 (7) (1993) 1868–1873.

[17] C.T. Gibson, D.A. Smith, C.J. Roberts, Calibration of silicon atomic force microscope cantilevers, Nanotechnology 16 (2) (2005) 234.
[18] M.S. Kim, J.H. Choi, J.H. Kim, Y.K. Park, Accurate determination of spring constant of atomic force microscope cantilevers and comparison with other methods, Measurement 43 (4) (2010) 520–526.
[19] D. Georgakaki, S. Mitridis, A.A. Sapalidis, E. Mathioulakis, H.M. Polatoglou, Calibration of tapping AFM cantilevers and uncertainty estimation: comparison between different methods, Measurement 46 (10) (2013) 4274–4281.
[20] Y. Song, S. Wu, L. Xu, X. Fu, Accurate calibration and uncertainty estimation of the normal spring constant of various AFM cantilevers, Sensors 15 (3) (2015) 5865–5883.
[21] See https://www.spmtips.com/afm-tip-hq-nsc14-al-bs.
[22] JCGM 100, Evaluation of Measurement Data — Guide to the Expression of Uncertainty in Measurement (GUM), Joint Committee for Guides in Metrology, 2008. Sévres, France.
[23] See https://www.digitalsurf.com/software-solutions/scanning-probe-microscopy/.
[24] N.T. Garabedian, H.S. Khare, R.W. Carpick, D.L. Burris, AFM at the macroscale: methods to fabricate and calibrate probes for millinewton force measurements, Tribol. Lett. 67 (2019) 1–10.
[25] Y. Tian, C. Zhou, F. Wang, K. Lu, D. Zhang, A novel compliant mechanism based system to calibrate spring constant of AFM cantilevers, Sensor Actuator Phys. 309 (2020) 112027.
[26] W.E. Newell, Miniaturization of Tuning Forks: integrated electronic circuits provide the incentive and the means for orders-of-magnitude reduction in size, Science 161 (3848) (1968) 1320–1326.
[27] T.R. Albrecht, S. Akamine, T.E. Carver, C.F. Quate, Microfabrication of cantilever styli for the atomic force microscope, J. Vac. Sci. Technol. A: Vacuum, Surfac. Film. 8 (4) (1990) 3386–3396.
[28] J.E. Sader, J. Sanelli, B.D. Hughes, J.P. Monty, E.J. Bieske, Distortion in the thermal noise spectrum and quality factor of nanomechanical devices due to finite frequency resolution with applications to the atomic force microscope, Rev. Sci. Instrum. 82 (9) (2011).
[29] J.E. Sader, J.R. Friend, Note: calibration of atomic force microscope cantilevers using only their resonant frequency and quality factor, Rev. Sci. Instrum. 85 (11) (2014).

Alessandro Schiavi[a,*], Luigi Ribotta[a], Luca Bruno[a,b], Marco Pisani[a], Roberto Bellotti[a], Massimo Zucco[a], Fabrizio Mazzoleni[a], Alessio Facello[a], Andrea Prato[a]

[a] *Istituto Nazionale di Ricerca Metrologica – INRiM (Applied Metrology and Engineering Division), Turin, Italy*

[b] *Politecnico di Torino (Mechanical Engineering), Turin, Italy*

[*] Corresponding author.

E-mail addresses: a.schiavi@inrim.it (A. Schiavi), s280287@studenti.polito.it (L. Bruno).